Resistive Instabilities in Reversed Shear Discharges and Wall Stabilization on JT-60U

S. Takeji, S. Tokuda, T. Fujita, T. Suzuki, A. Isayama, S. Ide, Y. Ishii, Y. Kamada, Y. Koide, T. Matsumoto, T. Oikawa, T. Ozeki, Y. Sakamoto, The JT-60 Team

Naka Fusion Research Establishment, Japan Atomic Energy Research Institute, 801-1 Mukoyama, Naka-machi, Ibaraki 311-0193, Japan

email contact of main author: takeji@naka.jaeri.go.jp

Abstract. Resistive instabilities and wall stabilization of ideal low toroidal mode number, n, kink modes are investigated in JT-60U reversed shear discharges. Resistive interchange modes with $n = 1$ are found to appear in reversed shear discharges with large pressure gradient at the normalized beta, $\beta_{\rm N}$, of about unity or even lower. The resistive interchange modes appear as intermittent burst-like magnetohydrodynamic (MHD) activities and higher $n \leq 3$ modes are observed occasionally in higher $\beta_{\rm N}$ regime. No clear degradation of the plasma stored energy is observed by the resistive interchange modes themselves. It is also found that resistive interchange modes can lead to major collapse owing to a coupling with tearing modes at the outer mode rational surface over the minimum safety factor. Stability analysis revealed that stability parameter of tearing modes, Δ', at the outer mode rational surface is affected by the free-boundary condition. The result is consistent with the experimental evidence that major collapse tends to occur when plasma edge safety factor, q^*, is near integer values. Stabilization of ideal low n kink modes by the JT-60U wall is demonstrated. Magnetohydrodynamic perturbations that are attributed to resistive wall modes are observed followed by major collapse in wall-stabilized discharges.

1 Introduction

A reversed shear discharge has inherent potential as an ultimate non-inductive steady-state tokamak operation since a reversed magnetic shear configuration can be consistent with large bootstrap current fraction [1]. Operation at high β is indispensable to generate large bootstrap current fraction. There exist a couple of crucial issues at a point of view of magnetohydrodynamic (MHD) stability to realize high β steady- state reversed shear discharges. One is to suppress resistive MHD instabilities which can cause serious problems in lower β regime than the ideal MHD stability limit. It is known that tearing modes appear to degrade the operational normalized beta, $\beta_{\rm N}$, in long pulse high β operation [2]. In addition to these tearing instabilities, other resistive instabilities such as resistive interchange modes [3] and double tearing modes [4] are also able to limit a tokamak operation with reversed shear configurations. The other is to improve the achievable β limit. Wall stabilization of low toroidal mode number, n, kink modes is crucial for significant improvement of stability and the operational β limit in reversed shear discharges since ideal MHD stability limits against low n kink modes are relatively lower in reversed shear configurations than that in conventional tokamak configurations [5].

In this paper, we describe resistive instabilities and influence to major collapse in JT-60U reversed shear discharges toward their steady-state high β operation. We also discuss issues concerning to wall stabilization by the JT-60U wall are reported.

2 Non-disruptive Resistive Modes (Resistive Interchange Modes)

Burst-like MHD activities often emerged in reversed shear discharges with large pressure gradient, ∇p, typically at the normalized beta, $\beta_{\rm N} = \beta(I_{\rm p}/aB)^{-1}$ (%mT/MA), about unity or even lower. Waveforms of plasma parameters in a typical high performance reversed shear discharge are shown in (a) of Fig.1. Normalized beta is kept being lower than unity when the minimum safety factor, $q_{\rm min}$, and the edge safety factor, q_{95}, are crossing three and four, respectively, to avoid major collapse [6]. Heating power by neutral beam injection, $P_{\rm NBI}$, increases slightly at

$t \sim 6.14$s and $\beta_{\rm N}$ begins to increase again. Time evolution of magnetic perturbations in the same discharge is shown in (b) and (c) of Fig.1. Toroidal mode number, n, of the magnetic perturbations in the frequency range of $f \sim 17$ kHz was identified to be $n = 1$ and the poloidal mode number, m, seemed to be $m = 3$. The burst-like activity with $n = 1$ appeared more clearly when $\beta_{\rm N}$ increased further. Growth time of the $n = 1$ burst-like mode is typically $\gamma^{-1} \sim 0.3$ ms which is that of resistive instabilities. Magnetic perturbations with $n = 2$ and $n = 3$ were also observed after that in the frequency range of twice and three times as high as that of $n = 1$. The gradual increase in the mode frequencies of $n = 1$, 2 and 3 seems to correspond to increase in the plasma rotation velocity due to increased $P_{\rm NBI}$. No clear in-out asymmetry was observed on the amplitude of magnetic perturbations by the burst-like MHD activities.

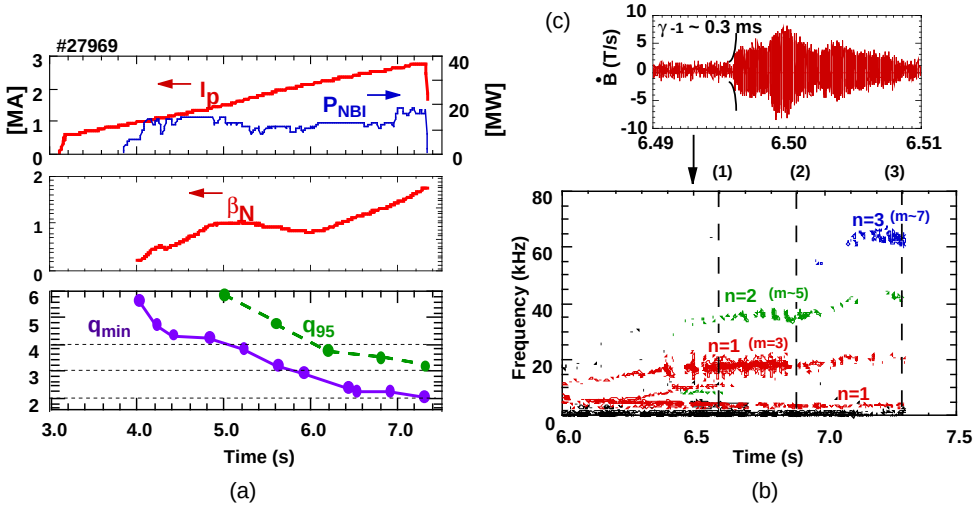

Figure 1. Time evolution of (a) plasma current I_p, neutral beam injection power, $P_{\rm NBI}$, normalized β, $\beta_{\rm N}$, minimum safety factor, $q_{\rm min}$, safety factor at the 95% flux surface, q_{95}, and (b) a contour map of power spectra of magnetic perturbations in a typical high performance reversed shear discharge with an L-mode edge. A waveform of magnetic perturbations around $t = 6.5$ s is shown in (c). Here, the origin of the horizontal axis ($t = 0$ s) is the starting time of the I_p build-up sequence. In the case of reversed shear discharges, I_p is build at $t \sim 3.1$ s in the practical manner due to a particular operational restriction on JT-60U.

Power spectrum densities (p.s.d.) of magnetic perturbations at time slots indicated as (1), (2) and (3) in (b) of Fig.1 are shown in (a), (b) and (c) of Fig.2, respectively. A strong $n = 1$ mode was observed at $t = 6.6$s and other n modes were much smaller than $n = 1$ ((a) of Fig.2). After that, an $n = 2$ mode appeared together with an $n = 1$ mode with larger amplitude than that of the $n = 1$ mode ((b) of Fig.2). Then, an $n = 3$ mode appeared together with $n = 1$ and 2 modes with relatively larger amplitude than those of $n = 1$ and $n = 2$ modes ((c) of Fig.2).

These burst-like activities were also measured on electron temperature, $T_{\rm e}$, perturbations measured by an electron cyclotron emission, ECE, diagnostic system. Radial location where the burst-like MHD activities occur can be identified through observation of $T_{\rm e}$ perturbations (Fig.3). It was found that these burst-like activities are localized radially in the negative magnetic shear region with large ∇p generated by the internal transport barrier. In this discharge, the radial location of the large ∇p moved outward together with that of $q_{\rm min}$. Mode rational surfaces on which large ∇p is formed moved in time from $m/n = 3/1$ to $m/n = 7/3$ through $m/n = 5/2$. Time evolution of observed mode number m/n can be attributed to the gradual change of the pressure and q profiles. Detailed observations of $T_{\rm e}$ perturbations with higher spatial resolution revealed no evidence of magnetic islands near the mode rational surface. We also confirmed by employing a reconstructed experimental equilibrium that stability criterion of the resistive interchange mode $D_{\rm R}$ [7] is violated ($D_{\rm R} > 0$), and ideal low n ($n = 1, 2$ and 3) kink modes and high n ballooning modes are stable. Therefore, the localized burst-like MHD activities are

identified as the resistive interchange instabilities. Resistive interchange modes in high temperature tokamak plasma was reported in the negative central magnetic shear discharges in DIII-D as a triggering event of disruption [3]. Direct observation of localized MHD perturbations of resistive interchange modes is, however, for the first time. The resistive interchange modes appeared as radially localized intermittent bursts and no clear degradation was observed by the burst-like activities themselves on the global plasma performance such as plasma stored energy.

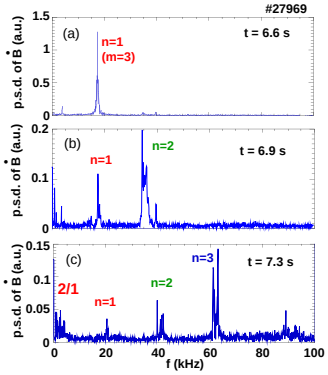

Figure 2. Power spectrum densities (p.s.d.) of magnetic perturbations in the discharge shown in Fig.1. Here, figures (a), (b) and (c) are p.s.d. at the time (1), (2) and (3) denoted in Fig. 1 (b), respectively.

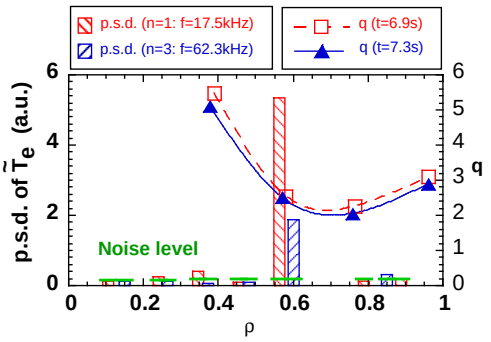

Figure 3. Radial distributions of p.s.d. of $n = 1$ and $n = 3$ components of $T_{\rm e}$ perturbations. Each of $n = 1$ and $n = 3$ components are calculated form $T_{\rm e}$ data for $6.8 \geq t \geq 6.85$s and $7.27 \geq t \geq 7.29$s, respectively. Safety factor profiles at $t = 6.8$s and $t = 7.3$ are also shown as a broken line with open squares and a solid line with closed triangles, respectively.

3 Disruptive Resistive Instabilities

Understanding of instabilities which relate to major collapse or disruption in reversed shear discharges is important for improvement of the attainable $\beta_{\rm N}$ and for the steady-state sustainment. Stability analysis of JT-60U's reversed shear discharges had been carried out at a point of view of ideal MHD [8, 9]. Reversed shear discharges in JT-60U are, however, often terminated in major collapse or disruption in the lower β regime than the expected ideal β limit, while upper limit of the achievable $\beta_{\rm N}$ is in agreement with the calculated no-wall ideal limit, $\beta_{\rm N}^{\rm no-wall}$ [8, 10]. Resistive MHD instabilities which closely relate to major collapse in the lower β regime are investigated in this section.

3.1 Experimental Observation

Time evolution of electron temperatures during a process of a major collapse in low β regime is shown in Fig.4. The plasma parameters just before the collapse are $\beta_{\rm N} = 0.77$, $q_{\rm min} = 2.1$ and $q^* = 4.85$. Here, q^* is a safety factor near the plasma edge and is defined as $q^* = (5a^2 B_{\rm T}/2RI_{\rm p}[1 + \kappa^2(1 + 2\delta^2 - 1.2\delta^3)]$ (B_T: toroidal magnetic field, R: major radius, κ: elongation, δ: triangularity). A difference in value between q^* and the safety factor at the 95% of the poloidal flux, q_{95}, is usually less than several percent of q^*. A thermal quench occurs at 6.1083 s. Electron temperature inside $\rho \sim 0.5$ decreases and $T_{\rm e}$ outside $\rho \sim 0.5$ increases abruptly by the thermal quench. The $T_{\rm e}$ evolves with $m/n = 3/1$ magnetic perturbations after the first thermal quench. Electron temperature perturbations showing existence of magnetic islands (phase inversion) was observed in similar discharges before the second thermal quench. The oscillation of $T_{\rm e}$ comes to a stop after the second thermal quench at 6.111 s, then $T_{\rm e}$ drops drastically everywhere by the last thermal quench at 6.1133 s.

Figure 5 shows radial profiles of $T_{\rm e}$, q, and $T_{\rm e}$ perturbations just before the first thermal quench at $\beta_{\rm N} = 0.77$ ($\beta_{\rm p} = 0.70$, $q^* = 4.85$). Perturbations of $T_{\rm e}$ with the growth time $\gamma^{-1} \sim 0.5$ms

appeared at the large ∇T_e region ($4 \sim 6$ ch) near the inner $q = 3$ surface with no clear evidence of magnetic islands. Perturbations of an $n = 1$ tearing mode (the estimated island width ~ 3 cm) were also observed on T_e near the outer $q = 3$ surface ($10 \sim 11$ ch). No clear perturbations were observed between these channels (7∼9ch) even just before the first thermal quench. After the first thermal quench, T_e profile changed drastically near the large ∇T_e region, then the change of T_e profile extended to the outer $q = 3$ surface.

We found the following remarkable features from Figs.4 and 5. One is that T_e perturbations on 10ch and 11ch is due to $n = 1$ tearing modes at the outer $q = 3$ surface. The other is that T_e perturbations at the large ∇T_e region (4∼6ch) and at the outer $q = 3$ surface (10ch, 11ch) oscillate with the same frequency for last two cycles just before the first thermal quench. The oscillation frequency looks different between them before the last two cycles. The matching behavior of the oscillation frequency between spatially separated modes suggests a mode coupling of an inner mode (a resistive mode at the large ∇T_e region) to a tearing mode at the outer $q = 3$ surface is a causal mechanism of the thermal quench.

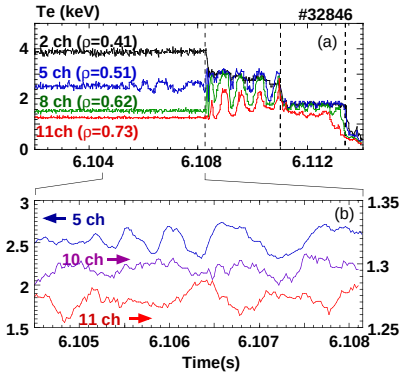

Figure 4. (a) Time evolution of electron temperature, T_e, in the process of a major collapse. A clear precursor appears just before the first thermal quench at 5 ch ($\rho = 0.51$). The first thermal quench is followed by larger amplitude T_e perturbations with $m/n = 3/1$. (b) Expanded waveforms of T_e right before the first thermal quench. Signals on 10ch ($\rho = 0.69$) and 11ch ($\rho = 0.73$) of which phase are inverted each other suggest existence of X-points of magnetic islands between them.

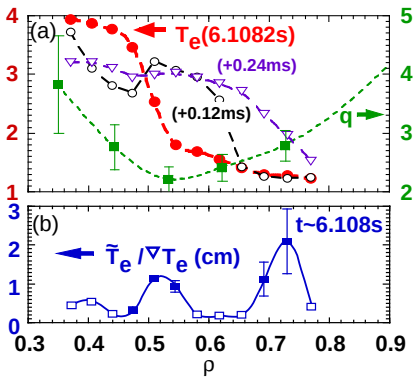

Figure 5. Radial profiles of (a) electron temperature T_e, q, and (b) amplitude of T_e perturbation $\tilde{T}_e$ normalized by the gradient of T_e, $\tilde{T}_e/\nabla T_e$ just before the first thermal quench. Here, closed squares show ECE channels on which obvious perturbations were observed, while open ones show ECE channels on which observed perturbations were in the noise level.

3.2 Stability Analysis

Stability analysis was carried out for the discharge discussed in Figs.4 and 5. Figure 6 shows eigenfunctions of a stable ideal mode calculated by the MARG2D code [11] in the free boundary condition. The linear stability code MARG2D can calculate Δ' including the effects of finite β, toroidal geometry and the free boundary condition. It is found that a stability parameter of tearing modes, Δ', is positive (destabilizing) only at the outer $q = 3$ surface ($\Delta'_{3,\mathrm{out}} > 0$) and Δ' at any other mode rational surfaces with respect to $n = 1$ such as $q = 4$ and $q = 5$ were negative (tearing modes are stable). These numerical results are consistent with the experimental evidence.

Moreover, stability parameter of double tearing modes, $\Delta(0)$, which is a rough evaluation by taking coupling between two mode rational surfaces on the same q value into account, is found to be negative (negative means destabilizing) only at the $q = 3$ surface. The numerical result suggests that double tearing modes could be a possible instability in the situation. On the other hand, it is also found that the stability criterion of resistive interchange modes is slightly broken ($D_R > 0$) near the inner $q = 3$ surface. Resistive interchange modes can also be unstable in the

experimental situation.

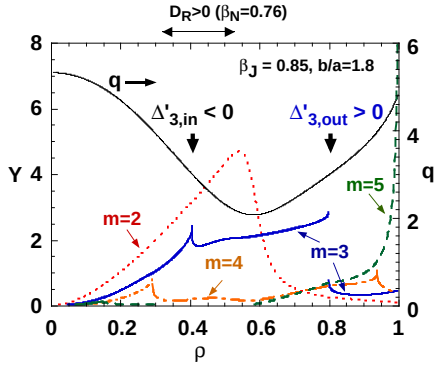

Figure 6. Eigenfunctions of $m = 2 \sim 5$ ($n = 1$) modes calculated by the MARG2D code in the free boundary condition ($d/a = 1.8$). A q-profile employed in this analysis is also shown as a solid line. Here, $\beta_{\rm N} = 1.11$ and $q_{\rm edge} \sim 4.87$.

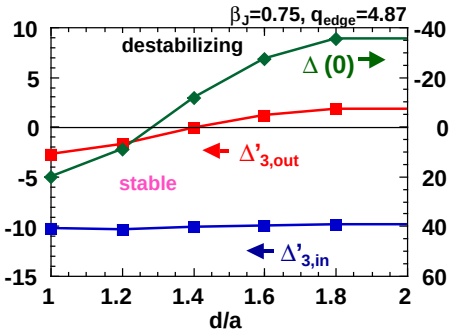

Figure 7. Dependence of stability parameter Δ' and $\Delta(0)$ on the wall position d/a. Here, $\Delta'_{3,\rm in}$ and $\Delta'_{3,\rm out}$ are Δ' at the inner and outer $q = 3$ rational surface, respectively.

4 Wall Stabilization Experiments

Wall stabilization of ideal low n kink modes is a key issue to demonstrate high β reversed shear discharges toward the steady-sate operation with large bootstrap current fraction. Both of theoretical and experimental studies of wall stabilization have been intensively carried out for tokamak plasmas [12–14]. Experimental study of stabilizing effects of the JT-60U wall and resistive wall modes have been carried out to provide physics basis of wall stabilization from JT-60U. Results of wall stabilization experiments are discussed in this section.

4.1 Improvement of Stability by the JT-60U Wall

Typical plasma shapes of high performance discharges in JT-60U are shown in Fig.8. Experiments for improved confinement have been usually carried out by employing plasma shapes with high elongation ($\kappa \lesssim 1.8$) such that the plasma surface is distant from the outer wall to reduce the effect of the toroidal ripple ((a) and (b) in Fig.8). We employed plasma shapes such as (c) in Fig.8 to be $d/a \leq 1.3$ (d: wall radius, a: plasma minor radius) in the following wall stabilization experiments.

Plasma performance of reversed shear discharges are often limited by disruption or major collapse in the wide range of $\beta_{\rm N}$ as mentioned in the previous section. Figure 9 shows the values of $\beta_{\rm N}$ as a function of the edge safety factor q^* at the time of disruptions or major collapses in reversed shear discharges. In the case of plasma shapes with $d/a > 1.5$ (i.e., (a) and (b) in Fig.8), the achievable $\beta_{\rm N}$ is lower than 2.3 in the L-mode edge discharges, and the achievable $\beta_{\rm N}$ was improved up to 2.6 by getting an H-mode edge. One of the remarkable results is that the achievable $\beta_{\rm N}$ is improved further (more than 10 %) by employing plasma shapes with $d/a < 1.3$ ((c) in Fig.8). The significant improvement of the achievable $\beta_{\rm N}$ must be due to stabilizing effects of the JT-60U wall. In several discharges with $d/a < 1.3$, the achieved $\beta_{\rm N}$ exceeded an empirical β limit scaling that $\beta_{\rm N} \sim 4\ell_{\rm i}$ ($\ell_{\rm i}$: internal inductance).

The other remarkable result is that major collapses in the lower $\beta_{\rm N}$ region hardly occur in the case of discharges of $d/a < 1.3$. A possible reason is that resistive (tearing) instabilities which can relate to major collapse at low $\beta_{\rm N}$ are effectively stabilized by the wall. Actually, Δ' at the outer mode rational surface is affected by the wall position and can be changed positive to negative if the conducting wall is close enough to the plasma surface (Fig.7).

4.2 Observation of Resistive Wall Modes

Improvement of stability owing to a stabilizing effect of the JT-60U wall was demonstrated as referred to above. Here, MHD instabilities observed in such wall stabilized discharges are described. Figure 10 shows waveforms of a reversed shear discharge in which the achieved $\beta_{\rm N}$ exceeded the calculated stability limit of the $n = 1$ ideal kink mode with the wall at infinity. The plasma volume is 77 $\rm m^3$ and $d/a \lesssim 1.3$. The calculated no-wall ideal stability limit is $\beta_{\rm N}^{\rm no-wall} \sim 2.2$ in the similar discharge with $\ell_{\rm i} \sim 0.7$. The normalized β increased gradually in time and exceeded $\beta_{\rm N}^{\rm no-wall}$ at $t \sim 6$ second. The discharge terminated in disruption at $\beta_{\rm N} = 2.6$. A set of eight saddle loops located toroidally at the mid-plane inside the vacuum vessel detected magnetic perturbations with $n = 1$ right before the disruption. Growth rate of the $n = 1$ mode is 120 $\rm s^{-1}$ which is corresponding to $\tau_{\rm w}^{-1}$. Any other mode numbers such as $n = 2$ and $n = 3$ were not observed at the same time. Plasma rotation frequency in the toroidal direction, f_{tor}, is about 4 kHz in the counter-direction to the plasma current at the radial region corresponding to $q = 3$ and $q = 4$ rational surfaces. The time resolution of the plasma rotation measurement by means of the charge exchange recombination spectroscopy is 16.7 ms. No significant change was not observed on f_{tor} near the outer $q = 3$ and $q = 4$ surfaces until beginning of the growth of the $n = 1$ mode. Change of f_{tor} during the growth of the $n = 1$ mode could not be observed owing to limitation of the time resolution.

A contour plot of the perturbed radial magnetic field shown in Fig.11 reveals an $n = 1$ mode rotating at the frequency $f \sim 20{\rm Hz} \sim 1/(2\pi\tau_{\rm w})$ in the counter-direction of the plasma current (the same direction with the plasma rotation). A growing $n = 1$ mode exists with the rotation frequency of $f \sim 20$ Hz. The MHD characteristics of the $n = 1$ mode appeared in the condition that $\beta_{\rm N} \geq \beta_{\rm N}^{\rm no-wall}$ is almost the same with that of *resistive wall modes* (RWMs) predicted theoretically [12] and reported experimentally on DIII-D [14]. Thus, the observed MHD perturbation is attributed to RWMs.

One of the differences of resistive wall modes in JT-60U from that reported in DIII-D is that no clear reduction of the plasma toroidal rotation velocity is observed near the mode rational surfaces (q = 3 and 4), while the toroidal rotation velocity is ~ 4 Hz before appearance of the RWMs in JT-60U. In the case of DIII-D, significant reduction of the plasma rotation velocity was observed when RWMs begun to grow [14]. The experimental evidence of the relation between the RWM amplitude and the reduction of the rotation frequency supports a theory in which torque balance is taken into account to determine plasma rotation self-consistently [13].

5 Summary and Conclusions

Magnetohydrodynamic stability was studied in discharges with negative central magnetic shear, i.e., reversed shear, configurations in JT-60U and the following results are obtained.

First, resistive interchange modes with $n = 1$ are found to appear in reversed shear discharges with large pressure gradient at the normalized β, $\beta_{\rm N}$, of about unity or even lower. The resistive interchange modes appear as intermittent burst-like MHD activities and higher $n \leq 3$ modes are also observed occasionally in higher $\beta_{\rm N}$ regime. Since resistive interchange modes are radially localized, no clear degradation of global plasma parameters such as the stored energy were observed by appearance of the resistive interchange modes themselves.

Second, resistive MHD instabilities which give rise to major collapse are studied. Experimental observations of MHD perturbations in the process of major collapse revealed that major collapse occurs by a coupling of a resistive mode near the inner mode rational surface to a tearing mode at the outer mode rational surface over the minimum safety factor. Linear stability analysis using the MARG2D code, which can evaluate Δ' under finite β, toroidal geometry and the free

boundary condition, showed that Δ' only at the outer $q = 3$ surface is positive (destabilizing). Roughly estimated stability parameter of double tearing modes, $\Delta(0)$, was negative (negative means destabilizing this case) at the $q = 3$ mode surfaces under the experimental condition. It was, however, also found that the stability criterion of resistive interchange modes is broken near the inner $q = 3$ surface. Mode structures observed in the experiments suggest that major collapse is owing to a coupling of a resistive interchange mode at the inner mode rational surface with a tearing mode at the outer mode rational surface. Resistive interchange modes can be disruptive under existence of tearing modes with certain size of magnetic islands.

Third, wall stabilization by the JT-60U wall was investigated. We confirmed that achievable $\beta_{\rm N}$ is limited at the ideal stability limit with no-wall $\beta_{\rm N}^{\rm no-wall}$ when the plasma surface is far from the wall ($d/a > 1.5$). When the wall is close enough to plasma surface (typically, $d/a < 1.3$), both of resistive and ideal modes can be stabilized by the wall and relatively higher β was obtained. Magnetohydrodynamic perturbations which have a growth rate of $\gamma \sim 1/\tau_{\rm w}$ with the toroidal rotation frequency $f \sim 1/(2\pi\tau_{\rm w})$ were observed in wall stabilized high β discharges. These MHD perturbations can be attributed to the resistive wall mode. Plasma rotation frequency f_{tor} near the mode rational surfaces of the outer $q = 3$ or $q = 4$ surfaces was ~ 4 kHz in the high β phase and no clear reduction was observed in the plasma rotation frequency when the resistive wall mode appeared.

Acknowledgements

The authors are grateful to Drs. M. Okabayashi and J. Manickam for discussion on stability of reversed shear discharges and wall stabilization experiments on JT-60U in collaboration between JAERI and the Princeton Plasma Physics Laboratory. The authors are also grateful to Prof. M. Wakatani, Prof. Z. Yoshida and Dr. T. Tatsuno for their theoretical suggestions. One of the authors (S.T.) is thankful to Dr. E.J. Strait and the DIII-D team for the opportunity to participate in resistive wall mode experiments in DIII-D. The authors also appreciate Ms. T. Ishizawa for her assistance for stability analysis using the MARG2D code.

References

[1] Ozeki, T., et al., in *Plasma Physics and Controlled Nuclear Fusion Research*, Würzburg, 1992 (IAEA, Vienna, 1993), Vol.2 p187.
[2] Sauter, O., et al., Phys. Plasmas **4** (1997) 1654.
[3] Chu, M.S., et al., Phys. Rev. Lett. **77** (1996) 2710.
[4] Chang, Z., et al., Phys. Rev. Lett. **77** (1996) 3553.
[5] Manickam, J., et al., Phys. Plasma **1** (1994) 1601.
[6] Fujita, T., et al., Nucl. Fusion **39** (1999) 1627, Fujita, T., et al., Nucl. Fusion **38** (1998) 207.
[7] Glasser, A., et al., Phys. Plasmas **18** (1975) 875.
[8] Ishii, Y., et al., Plamsa Phys. Control. Fusion **40** (1998) 1067.
[9] Manickam, J., et al., Nucl. Fusion **39** (1999) 1819.
[10] Takeji, S., et al., J. Plasma Fusion Res. **76** (2000) 575.
[11] Tokuda, S., Watanabe, T., Phys. Plasmas **6** (1999) 3012.
[12] Bondeson, A., Ward., D.J., Phys. Rev. Lett. **72** (1984) 2709.
[13] Gimblett, C.G., Hastie, R.J., Phys. Plasmas **7** (2000) 258.
[14] Strait, E.J., et al., Nucl. Fusion **39** (1999) 1977, Garofalo, A.M., et al., Nucl. Fusion **40** (2000) 1491 and papers cited therein.

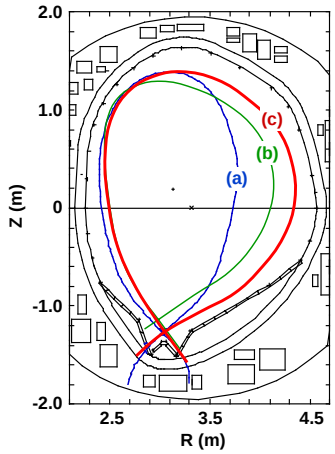

Figure 8. Typical plasma shapes of reversed shear discharges in JT-60U. (a): High elongation ($\kappa \sim 1.8$) for stability at high plasma current, (b): high triangularity ($\delta \geq 0.3$) for improved edge stability and (c): large volume ($V_{\rm p} \sim 75{\rm m}^3$) with $d/a \sim 1.3$ for wall stabilization.

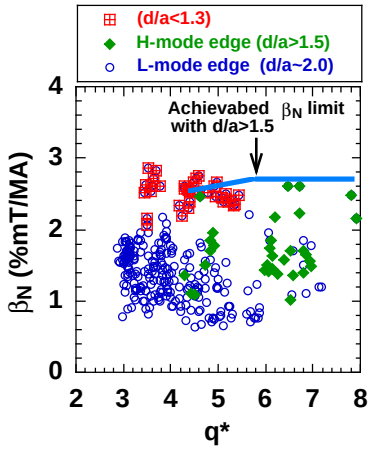

Figure 9. Normalized β, $\beta_{\rm N}$, versus edge safety factor q^* at the time of disruptions or major collapses in several type of JT-60U reversed shear discharges. Open circles are data of the L-mode edge discharges with the plasma shape (a) in Fig.8. Closed diamonds are ones of the highest $\beta_{\rm N}$ data obtained in discharges with the H-mode edge with the plasma shape (a) or (b) in Fig.8. Squares are ones obtained in discharges with $d/a \leq 1.3$ ((c) in Fig.8).

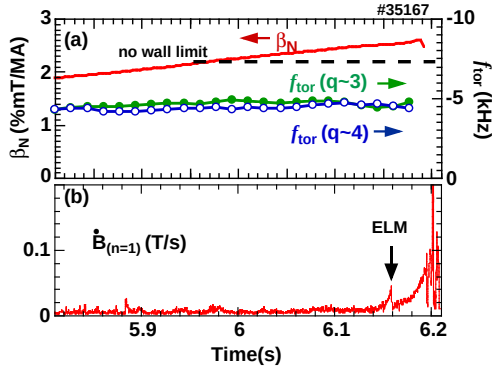

Figure 10. Waveforms of (a) $\beta_{\rm N}$ and plasma rotation frequency in the toroidal direction $f_{\rm tor}$ at $q \sim 3$ and ~ 4, (b) time derivative of $n = 1$ radial magnetic perturbations.

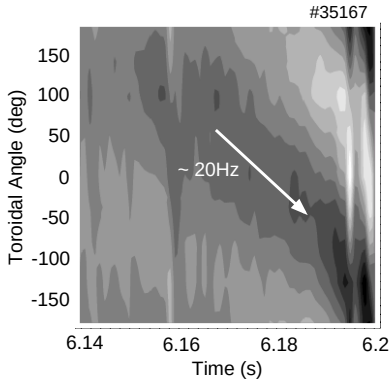

Figure 11. Contour plot of time derivative of the perturbed radial magnetic field measured by the toroidal array of saddle loop sensors inside the vessel.